

Dear Author,

Here are the proofs of your article.

- You can submit your corrections **online**, via **e-mail** or by **fax**.
- For **online** submission please insert your corrections in the online correction form. Always indicate the line number to which the correction refers.
- You can also insert your corrections in the proof PDF and **email** the annotated PDF.
- For fax submission, please ensure that your corrections are clearly legible. Use a fine black pen and write the correction in the margin, not too close to the edge of the page.
- Remember to note the **journal title**, **article number**, and **your name** when sending your response via e-mail or fax.
- **Check** the metadata sheet to make sure that the header information, especially author names and the corresponding affiliations are correctly shown.
- **Check** the questions that may have arisen during copy editing and insert your answers/ corrections.
- **Check** that the text is complete and that all figures, tables and their legends are included. Also check the accuracy of special characters, equations, and electronic supplementary material if applicable. If necessary refer to the *Edited manuscript*.
- The publication of inaccurate data such as dosages and units can have serious consequences. Please take particular care that all such details are correct.
- Please **do not** make changes that involve only matters of style. We have generally introduced forms that follow the journal's style. Substantial changes in content, e.g., new results, corrected values, title and authorship are not allowed without the approval of the responsible editor. In such a case, please contact the Editorial Office and return his/her consent together with the proof.
- If we do not receive your corrections **within 48 hours**, we will send you a reminder.
- Your article will be published **Online First** approximately one week after receipt of your corrected proofs. This is the **official first publication** citable with the DOI. **Further changes are, therefore, not possible.**
- The **printed version** will follow in a forthcoming issue.

Please note

After online publication, subscribers (personal/institutional) to this journal will have access to the complete article via the DOI using the URL: [http://dx.doi.org/\[DOI\]](http://dx.doi.org/[DOI]).

If you would like to know when your article has been published online, take advantage of our free alert service. For registration and further information go to: <http://www.link.springer.com>.

Due to the electronic nature of the procedure, the manuscript and the original figures will only be returned to you on special request. When you return your corrections, please inform us if you would like to have these documents returned.

Metadata of the article that will be visualized in OnlineFirst

ArticleTitle	Impact of protein–ligand solvation and desolvation on transition state thermodynamic properties of adenosine A _{2A} ligand binding kinetics	
--------------	--	--

Article Sub-Title		
-------------------	--	--

Article CopyRight	Springer-Verlag GmbH Germany, part of Springer Nature (This will be the copyright line in the final PDF)	
-------------------	---	--

Journal Name	In Silico Pharmacology	
--------------	------------------------	--

Corresponding Author	Family Name	Deflorian
	Particle	
	Given Name	Francesca
	Suffix	
	Division	
	Organization	Heptares Therapeutics Ltd.
	Address	BioPark, Broadwater Road, Welwyn Garden City, Herts, AL7 3AX, UK
	Phone	+44(0)1707 358646
	Fax	
	Email	francesca.deflorian@heptares.com
	URL	

Author	Family Name	Deganutti
	Particle	
	Given Name	Giuseppe
	Suffix	
	Division	Molecular Modeling Section (MMS), Department of Pharmaceutical and Pharmacological Sciences
	Organization	University of Padova
	Address	Via Marzolo 5, Padua, Italy
	Phone	
	Fax	
	Email	
	URL	

Author	Family Name	Zhukov
	Particle	
	Given Name	Andrei
	Suffix	
	Division	
	Organization	Heptares Therapeutics Ltd.
	Address	BioPark, Broadwater Road, Welwyn Garden City, Herts, AL7 3AX, UK
	Phone	
	Fax	
	Email	

URL
ORCID

Author	Family Name	Federico
	Particle	
	Given Name	Stephanie
	Suffix	
	Division	Department of Chemical and Pharmaceutical Sciences
	Organization	University of Trieste
	Address	Piazzale Europa, 34127, Trieste, Italy
	Phone	
	Fax	
	Email	
	URL	
	ORCID	

Author	Family Name	Spalluto
	Particle	
	Given Name	Giampiero
	Suffix	
	Division	Department of Chemical and Pharmaceutical Sciences
	Organization	University of Trieste
	Address	Piazzale Europa, 34127, Trieste, Italy
	Phone	
	Fax	
	Email	
	URL	
	ORCID	

Author	Family Name	Cooke
	Particle	
	Given Name	Robert M.
	Suffix	
	Division	
	Organization	Heptares Therapeutics Ltd.
	Address	BioPark, Broadwater Road, Welwyn Garden City, Herts, AL7 3AX, UK
	Phone	
	Fax	
	Email	
	URL	
	ORCID	

Author	Family Name	Moro
	Particle	
	Given Name	Stefano
	Suffix	
	Division	Molecular Modeling Section (MMS), Department of Pharmaceutical and Pharmacological Sciences
	Organization	University of Padova

Address Via Marzolo 5, Padua, Italy
Phone
Fax
Email
URL
ORCID

Author	Family Name	Mason
	Particle	
	Given Name	Jonathan S.
	Suffix	
	Division	
	Organization	Heptares Therapeutics Ltd.
	Address	BioPark, Broadwater Road, Welwyn Garden City, Herts, AL7 3AX, UK
	Phone	
	Fax	
	Email	
	URL	
	ORCID	

Author	Family Name	Bortolato
	Particle	
	Given Name	Andrea
	Suffix	
	Division	
	Organization	Heptares Therapeutics Ltd.
	Address	BioPark, Broadwater Road, Welwyn Garden City, Herts, AL7 3AX, UK
	Phone	
	Fax	
	Email	
	URL	
	ORCID	

Schedule	Received	10 August 2017
	Revised	
	Accepted	14 November 2017

Abstract Ligand–protein binding kinetic rates are growing in importance as parameters to consider in drug discovery and lead optimization. In this study we analysed using surface plasmon resonance (SPR) the transition state (TS) properties of a set of six adenosine A_{2A} receptor inhibitors, belonging to both the xanthine and the triazolo-triazine scaffolds. SPR highlighted interesting differences among the ligands in the enthalpic and entropic components of the TS energy barriers for the binding and unbinding events. To better understand at a molecular level these differences, we developed suMetaD, a novel molecular dynamics (MD)—based approach combining supervised MD and metadynamics. This method allows simulation of the ligand unbinding and binding events. It also provides the system conformation corresponding to the highest energy barrier the ligand is required to overcome to reach the final state. For the six ligands evaluated in this study their TS thermodynamic properties were linked in particular to the role of water molecules in solvating/desolvating the pocket and the small molecules. suMetaD identified kinetic bottleneck conformations near the bound state position or in the vestibule area. In the first case the barrier is mainly enthalpic, requiring the breaking of strong interactions with the protein. In the vestibule TS location the kinetic bottleneck is instead mainly of entropic nature, linked to the solvent behaviour.

Keywords (separated by '-') Metadynamics - Supervised molecular dynamics - Ligand binding kinetics - SPR - Biacore - Molecular dynamics

Footnote Information **Electronic supplementary material** The online version of this article (<https://doi.org/10.1007/s40203-017-0037-x>) contains supplementary material, which is available to authorized users.

Metadata of the article that will be visualized in OnlineAlone



2 Impact of protein–ligand solvation and desolvation on transition state 3 thermodynamic properties of adenosine A_{2A} ligand binding kinetics

4 Giuseppe Deganutti¹ · Andrei Zhukov² · Francesca Deflorian² · Stephanie Federico³ · Giampiero Spalluto³ ·
5 Robert M. Cooke² · Stefano Moro¹ · Jonathan S. Mason² · Andrea Bortolato²

6 Received: 10 August 2017 / Accepted: 14 November 2017
7 © Springer-Verlag GmbH Germany, part of Springer Nature 2017

8 Abstract

9 Ligand–protein binding kinetic rates are growing in importance as parameters to consider in drug discovery and lead opti-**AQ1**
10 mization. In this study we analysed using surface plasmon resonance (SPR) the transition state (TS) properties of a set of
11 six adenosine A_{2A} receptor inhibitors, belonging to both the xanthine and the triazolo-triazine scaffolds. SPR highlighted
12 interesting differences among the ligands in the enthalpic and entropic components of the TS energy barriers for the binding
13 and unbinding events. To better understand at a molecular level these differences, we developed suMetaD, a novel molecu-
14 lar dynamics (MD)—based approach combining supervised MD and metadynamics. This method allows simulation of the
15 ligand unbinding and binding events. It also provides the system conformation corresponding to the highest energy barrier
16 the ligand is required to overcome to reach the final state. For the six ligands evaluated in this study their TS thermodynamic
17 properties were linked in particular to the role of water molecules in solvating/desolvating the pocket and the small molecules.
18 suMetaD identified kinetic bottleneck conformations near the bound state position or in the vestibule area. In the first case
19 the barrier is mainly enthalpic, requiring the breaking of strong interactions with the protein. In the vestibule TS location
20 the kinetic bottleneck is instead mainly of entropic nature, linked to the solvent behaviour.

21 **Keywords** Metadynamics · Supervised molecular dynamics · Ligand binding kinetics · SPR · Biacore · Molecular
22 dynamics

23 Introduction

24 The importance of the pharmacology of adenosine receptors
25 (ARs) is daily experienced by millions of coffee drinkers
AQ2 26 worldwide. Indeed, it is well established that caffeine is able
27 to non-selectively inhibit AR subtypes (Rivera-Oliver and
Díaz-Ríos 2014) (A₁, A_{2A}, A_{2B} and A₃) leading to a range of

different biological responses and suggesting the potential
28 usefulness of AR agonists or blocking agents (Jacobson and
29 Gao 2006; Polosa and Blackburn 2009; Stone et al. 2009).
30 Increasing attention is being addressed to the A_{2A} AR and
31 its modulation due to its emerging value in multiple disease
32 states: Parkinson's disease (Richardson et al. 1997), mainly
33 attributed to the heterodimerization with the dopamine
34 receptor D₂ in the central nervous system (CNS) striatum
35 (Fink et al. 1992), attention deficit hyperactivity disorder
36 (ADHD) and immuno-oncology. The A_{2A} AR represents a
37 good starting point for structure-based drug design (SBDD)
38 among all the G protein-coupled receptors (GPCRs) super-
39 family members. Despite the intrinsic difficulties of GPCR
40 crystallography (Ghosh et al. 2015), to date 20 X-ray struc-
41 tures of the A_{2A} AR have already been published, in complex
42 with both agonists (Lebon et al. 2011, 2015; Xu et al. 2011),
43 including a recent structure bound to an engineered G pro-
44 tein (Carpenter et al. 2016), and antagonists (Congreve et al.
45 2012; Doré et al. 2011; Hino et al. 2012; Jaakola et al. 2008;
46 Liu et al. 2012; Segala et al. 2016).
47
48

A1 **Electronic supplementary material** The online version of this
A2 article (<https://doi.org/10.1007/s40203-017-0037-x>) contains
A3 supplementary material, which is available to authorized users.

A4 ✉ Francesca Deflorian
A5 francesca.deflorian@heptares.com

A6 ¹ Molecular Modeling Section (MMS), Department
A7 of Pharmaceutical and Pharmacological Sciences, University
A8 of Padova, Via Marzolo 5, Padua, Italy

A9 ² Heptares Therapeutics Ltd., BioPark, Broadwater Road,
A10 Welwyn Garden City, Herts AL7 3AX, UK

A11 ³ Department of Chemical and Pharmaceutical Sciences,
A12 University of Trieste, Piazzale Europa, 34127 Trieste, Italy

49 Compared to the thermodynamic dissociation constant
50 K_D , binding kinetic rate constants k_{on} and k_{off} , are gaining
51 in importance as parameters to consider in drug discovery
52 and lead optimization. In fact, data obtained from in vitro
53 steady state conditions are not always predictive for the
54 in vivo biological environment, where the concentration of
55 a ligand in proximity of its endogenous target is governed
56 by pharmacokinetics (PK). As a consequence, increasing
57 efforts are being addressed to the development of reliable
58 structure-kinetic relationships (SKR), able to drive improve-
59 ments in the kinetic profile of potential drug candidates.
60 Indeed, compounds from a chemical series may show very
61 similar affinities but dissimilar kinetic behaviour (Guo et al.
62 2017). The dynamic properties of binding equilibria allow
63 the thermodynamic constant K_D to be related to the kinetic
64 rate constants k_{on} and k_{off} , as shown in Eq. (1)
65

$$K_D = \frac{k_{off}}{k_{on}}. \quad (1)$$

66 Drug-like compounds have k_{on} values generally in the
67 range of 10^3 – 10^9 $M^{-1} s^{-1}$ (the latter is approximately the
68 rate limit of free diffusion in solution), with k_{off} values rang-
69 ing from about 10^{-7} s^{-1} to approximately 1 s^{-1} (Copeland
70 2015). Interestingly, super-fast binders (e.g. characterized by
71 k_{on} larger than 10^9 $M^{-1} s^{-1}$) have been evolutionary selected
72 as effectors of physiologic processes that need instant regula-
73 tion, like acetylcholine on acetylcholinesterase (AChE)
74 (Radić et al. 1997) in the central nervous system (CNS).
75 Nowadays it is common to refer to the kinetic concept of
76 residence time (t_r), first introduced in 2006 (Copeland et al.
77 2006) and defined as the reciprocal of the k_{off} value (e.g.
78 $t_r = 1/k_{off}$); t_r is related to the in vivo biological effects trig-
79 gered by ligands (Copeland 2015; Hothersall et al. 2016).
80 The value of t_r , especially when longer than the pharma-
81 cokinetic elimination lifetime, is generally associated with
82 a favourable pharmacodynamic profile (Dahl and Akerud
83 2013) and may be important for tuning the agonist signal-
84 ling bias (Kenakin and Christopoulos 2012), an emerging
85 concept in GPCRs pharmacology. It is defined as the ability
86 of ligands to preferentially signal through different effec-
87 tors, triggering a distinct functional effect. Nevertheless, it is
88 necessary to consider that also adverse effects can be linked
89 to high t_r values (Vauquelin et al. 2012). The k_{on} has a cru-
90 cial role in the setup of protocols for binding measurements
91 (Hulme and Trevethick 2010), being the kinetic *on* rate of
92 ligands involved in the experimental procedures; it critically
93 drives the time needed to achieve the required equilibrium
94 conditions.

95 From a mechanistic point of view, there is a range of
96 driving forces that determine the free energy change dur-
97 ing molecular binding and unbinding transitions. These
98 include desolvation phenomena (Dror et al. 2011; Pan et al.

2013), conformational entropy loss (Frederick et al. 2007) 99
and favourable and unfavourable intermolecular interac- 100
tions (Radić et al. 1997; Schmidtke et al. 2011). The first 101
extracellular vestibules that ligands encounter are the extra- 102
cellular loops (ELs), excluding ligands able to reach the 103
GPCR orthosteric binding site by diffusing from the mem- 104
brane bilayer [as described by Stanley et al. (2016)]. These 105
structural elements can modulate kinetic rates (Guo et al. 106
2017; Segala et al. 2016) and selectivity profiles (Nguyen 107
et al. 2016; Seibt et al. 2013), mainly due to their intrin- 108
sic flexibility and high degree of structural variability. 109
Molecular dynamics (MD) simulations represent the best 110
computational approach for modeling events that are deeply 111
influenced by flexibility and water molecules. Indeed, MD— 112
based “enhanced sampling” methods are extensively used 113
to simulate transitions of chemical systems between energy 114
minima that are separated by high energy barriers and there- 115
fore associated with slow kinetic rates. This is the case for 116
ligand unbinding, where the time scale reaches up to several 117
hours or days, and is thus too computationally expensive for 118
a single unbiased MD simulation starting from the ligand 119
bound conformation; nowadays it is possible to reach the 120
millisecond time scale on specialized machines (Shaw et al. 121
2009). Kinetic descriptions of binding and unbinding have 122
been addressed by several different approaches, includ- 123
ing, but not limited to, methods introducing an energy bias 124
as a scalar in the potential energy equation of the system 125
(Fukunishi et al. 2002; Hamelberg et al. 2004; Luitz and 126
Zacharias 2014; Mollica et al. 2015, 2016; Pierce et al. 2012; 127
Sinko et al. 2013; Wang et al. 2013) and methods requir- 128
ing a preliminary definition of a set of collective variables 129
(CVs) to be biased during the simulation (Barducci et al. 130
2011; Bui et al. 2003; Gervasio et al. 2005; Guo et al. 2016; 131
Isralewitz et al. 2001; Laio and Parrinello 2002; Laio et al. 132
2005; Li 2005; Patel et al. 2014; Torrie and Valleau 1977; 133
Yu et al. 2016). CVs can be for example intermolecular or 134
interatomic distances, angles formed by atoms or group of 135
atoms, coordination numbers, degree of solvation and they 136
are used in order to drive the binding/unbinding transition 137
and to map the corresponding energy profile. Among them, 138
metadynamics (Barducci et al. 2011; Gervasio et al. 2005; 139
Laio and Parrinello 2002; Laio et al. 2005) is probably one 140
of the most used methods. During a metadynamics simula- 141
tion, a history-dependent energetic term (centred along the 142
pre-defined set of CVs) is added at discrete time intervals, 143
decreasing the probability that the system will revisit that 144
specific configuration and increasing the probability of a 145
transition from one trough to another one (e.g. the ligand in 146
the bound and unbound states, respectively) (Barducci et al. 147
2011). More recently, alternative metadynamics approaches 148
like adaptive Gaussian (Branduardi et al. 2012) and well 149
tempered metadynamics (WT-metaD) (Barducci et al. 2008, 150
2011) have been introduced. 151

152 Computational chemists are constantly working on new
153 tools to allow evaluation of ligand kinetics and rational-
154 ize experimental data. From this perspective, the aMetaD
155 protocol (Bortolato et al. 2015) was recently developed and
156 tested on three GPCR systems. This approach combines adi-
157 abatic-bias molecular dynamics (ABMD) (Marchi and Bal-
158 lone 1999) and WT-metaD in order to simulate ligand–pro-
159 tein unbinding events and provide an energy estimation of

160 predicted transition states. The output from aMetaD allows
161 rapid ranking of structurally related ligands according to
162 predicted unbinding energetics (e.g. slow off and fast off
163 compounds), as well as insights into the water dynamics dur-
164 ing the dissociation. However, the need for a more complete
165 ligand kinetics evaluation inspired us to develop a new pro-
166 tocol, capable of reconstructing an energy profile associated
167 to both the binding and unbinding events: starting from a
168 docked intermolecular complex. This MD—based sampling
169 method is able to consecutively simulate ligand unbinding
170 and binding, using a supervised MD (SuMD) approach
171 (Cuzzolin et al. 2016; Sabbadin and Moro 2014) and keep-
172 ing track of the energy required for the transition by mean
173 of metadynamics. The supervised metadynamics (suMetaD)
174 algorithm was tested on a set of A_{2A} AR antagonists (Fig. 1),
175 belonging to both the xanthine (XAC, DPCPX, KW3902)
176 and the [1,2,4]triazolo[1,5-*a*][1,3,5]triazine [ZM241385,
177 Z48 (Federico et al. 2011), Z80 (Federico et al. 2016)] scaf-
178 folds, whose transition state thermodynamics were experi-
179 mentally determined using the surface plasmon resonance
180 (SPR) technique (Fig. 2). The past 10 years have seen a sig-
181 nificant surge in the application of SPR technology to study
182 small molecule interactions; it uses a protein in real time
183 without labelling (Du et al. 2016; Rich and Myszk a 2009).
184 Engineering stabilized GPCRs allows SPR techniques to be
185 applied to this class of membrane receptors with promis-
186 ing results (Rich et al. 2011; Shepherd et al. 2014). Using

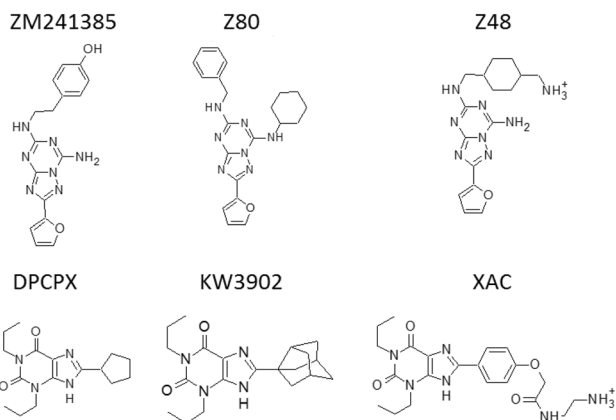


Fig. 1 Chemical structures of the A_{2A} AR ligands considered for the suMetaD test. ZM241385, Z80 and Z48 are [1,2,4]triazolo[1,5-*a*][1,3,5]triazine inhibitors; DPCPX, KW3902 and XAC are xanthine inhibitors

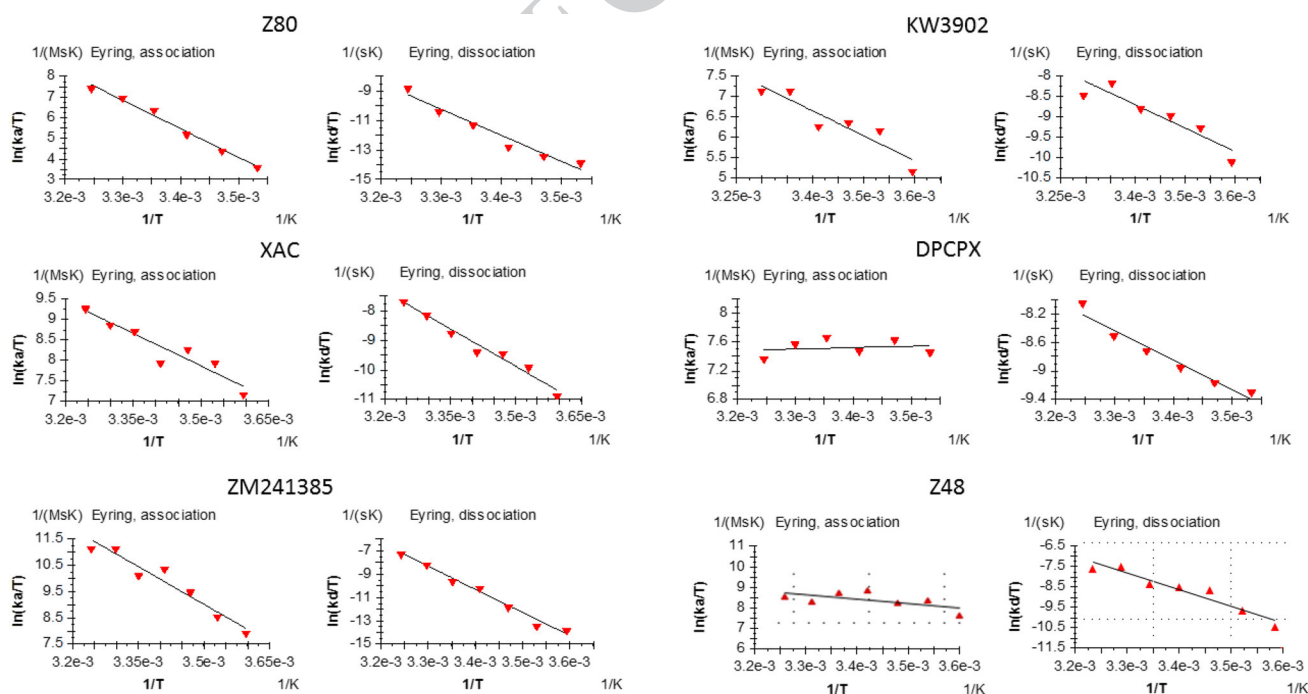


Fig. 2 Eyring equation plots for the ligand binding association (left) and dissociation (right) from the SPR analysis for the 6 ligands included in this study. The values for ΔH^\ddagger and ΔS^\ddagger can be determined

from kinetic data plotting $\ln(t/T)$ vs $1/T$. In the resulting linear interpolation equation the slope corresponds to $\Delta H^\ddagger/R$ and the ΔS^\ddagger can be calculated from the y-intercept

187 SPR to measure the affinity of interaction K_D at a series of
 188 temperatures allows the enthalpy ΔH° and entropy ΔS° of
 189 interaction to be calculated using the van't Hoff equation
 190 (here in its integrated form)

191
$$\ln K_D = \Delta H^\circ / RT - \Delta S^\circ / R,$$

192 where R is the universal gas constant. This approach has
 193 been used in a number of studies (Borea et al. 2004; Roos
 194 et al. 1998; Sahlan et al. 2010).

195 Likewise, measuring the rate constant k of association
 196 or dissociation as a function of temperature enables a crude
 197 approximation of the enthalpy ΔH^{\ddagger} and entropy ΔS^{\ddagger} of the
 198 transition state formation using the Eyring equation (here in
 199 its integrated form) to be obtained.

200
$$\ln \frac{k}{T} = -\Delta H^{\ddagger} / RT + \Delta S^{\ddagger} / R + \ln k_B / h,$$

201 where R is the universal gas constant, k_B is Boltzmann con-
 202 stant, and h is Planck's constant.

203 Studying the mechanism of transition state formation can
 204 provide important additional information helping to under-
 205 stand why interactions with similar affinities can have dif-
 206 ferent kinetics.

207 From this standpoint, the suMetaD computational proto-
 208 col allows to obtain insights into kinetic bottlenecks along
 209 the simulated pathways that offer a rationale for understand-
 210 ing experimental transition state (TS) thermodynamic data
 211 and allow generation of working hypotheses on the role of
 212 enthalpy and entropy during the binding and unbinding rate
 213 limiting steps.

214 Using SPR we evaluated the ligand binding and unbind-
 215 ing event to the A_{2A} AR stabilized receptor (StaRTM) for the
 216 6 ligands shown in Fig. 1. Transition state thermodynam-
 217 ics was evaluated using association and dissociation rate
 218 constants measured at temperatures between 5 and 35 °C at
 219 5 °C intervals. A series of five twofold dilutions of the test
 220 compounds was injected and the obtained sensorgrams were
 221 fitted to a 1:1 interaction model to obtain the rate constants.
 222 The temperature dependence of the rate constants was fitted

to Eyring equation using Biacore T200 evaluation software
 to obtain enthalpy and entropy of TS formation (Fig. 2).

Results

The obtained experimental transition state thermodynam-
 ics results are summarized in Table 1. It is interesting to
 note that the spread in the TS free energy for the test set is
 about 2.5 kcal/mol for both the association and dissociation
 events. The enthalpic and entropic components however
 have stark differences in the energy barriers: ΔH and $T\Delta S$
 cover a range of more than 20 kcal/mol for the binding event
 and more than 30 kcal/mol for the unbinding event. The
 smaller changes in ΔG^\ddagger among the ligands is the result of
 enthalpy–entropy compensation effects: higher ΔH^\ddagger energy
 barrier correspond to lower $-T\Delta S^\ddagger$ and vice versa.

To support the analysis of the experimental data we
 developed a novel computational protocol based on MD to
 study putative ligand unbinding and binding events. It is
 based on a supervised algorithm (Sabbadin and Moro 2014),
 that drives the exploration only of ligand–protein conforma-
 tions starting from a provided bound state conformation (SI
 Fig. 2) that are compatible with paths linking the orthos-
 teric site to the extracellular bulk solvent. It evaluates if the
 ligand is moving in the right direction, calculating the root
 mean square deviation (RMSD) of the ligand coordinates
 during the MD from the unbound (unbinding path) or bound
 (binding path) ligand target conformation. At the same time
 the relative free energy of the unbinding/binding paths are
 estimated using metadynamics (Barducci et al. 2011). Dur-
 ing the metadynamics simulation a history dependent bias
 is added to the potential energy landscape representing the
 unbinding and binding events. The analysis of the resulting
 energy profile (SI Fig. 3) allows the estimation of a repre-
 sentative protein–ligand conformation corresponding to the
 highest energy barrier the ligand has to overcome during
 its path toward the target positions. These conformations
 can be useful to understand at a molecular level the *on* and
off rate TS energy barriers linked to the ligand binding/

Table 1 Transition state thermodynamic results obtained from the SPR analysis of the association and dissociation of the six ligands considered in this study to the A_{2A} AR

	Association (kcal/mol)			Dissociation (kcal/mol)		
	ΔH^\ddagger	$-T\Delta S^\ddagger$	ΔG^\ddagger	ΔH^\ddagger	$-T\Delta S^\ddagger$	ΔG^\ddagger
ZM241385	19.1 ± 2.2	- 11.2 ± 2.2	7.9	40.6 ± 2.2	- 19.8 ± 2.2	20.8
XAC	10.5 ± 1.7	- 1.5 ± 1.7	9.0	16.7 ± 1.4	2.4 ± 1.4	19.1
DPCPX	- 0.4 ± 1.0	10.0 ± 1.0	9.6	8.4 ± 0.9	11.0 ± 0.9	19.4
KW3902	12.2 ± 2.4	- 2.2 ± 2.4	10.0	11.2 ± 2.3	7.7 ± 2.3	18.9
Z80	22.7 ± 1.8	- 12.4 ± 1.8	10.3	19.6 ± 1.8	- 1.4 ± 1.8	18.2
Z48	5.5 ± 1.4	3.6 ± 1.4	9.1	16.5 ± 2.5	2.3 ± 2.5	18.8

Association and dissociation rate constants were measured at temperatures between 5 and 35 °C at 5 °C intervals

260 unbinding kinetic bottlenecks. Movies with the simulations
261 of the unbinding/binding event for each ligand are available
262 as Supplementary Material (videos S1–S6).

263 Visual inspection of the representative kinetic bottlenecks
264 shows different location of the ligands in the predicted TS
265 complex conformation (Figs. 3, 4). During the binding event
266 the ligand faces ordered water molecules in the orthosteric
267 site, some creating stable favourable interactions with the
268 protein (Fig. 3). When the energy barrier is predicted to be
269 located near the vestibule region of the receptor, the ligand
270 generally does not need to displace tightly protein-bound
271 waters. This is in agreement with the resulting low enthalpic
272 energy barrier. In parallel, the solvent is trapped in the
273 orthosteric site by the ligand position in the vestibule area,
274 resulting in lower probability of exchange with bulk solvent
275 and a high entropic barrier to the binding event. For some
276 other ligands the energy barrier was predicted to correspond
277 to a ligand location deep in the pocket, close to the final
278 bound state. A high enthalpic barrier in this case is expected
279 to be linked to the required displacement of water molecules
280 in the orthosteric site tightly bounded to the protein. Their
281 release to bulk results in a favourable entropic gain linked
282 to the ligand binding event.

283 During the unbinding event the ligand faces a cap of
284 ordered water molecules in the orthosteric site and it has to
285 disrupt strong protein–ligand interactions (Fig. 4). Similar to
286 the analysis of the binding event, we predicted two possible
287 ligand locations corresponding to the unbinding transition

288 states: near the vestibule region or close to the bound state.
289 A kinetic bottleneck near the vestibule area and the extra-
290 cellular loops is characterized by a high entropic barrier
291 mainly linked to the solvation of non-polar ligand atoms.
292 In contrast, a low enthalpic barrier is the result of weaker
293 interactions with the protein in this region compared to when
294 the ligand is located deep in the orthosteric site. An unbind-
295 ing transition state close to the bound state conformation is
296 characterized by a high enthalpic barrier related to strong
297 interactions with the receptor. In this case the unbinding
298 event starts from a complex conformation where the waters
299 are tightly bound to the protein and/or to the small molecule,
300 evolving into a nearby TS conformation where they are more
301 disordered (resulting in a low entropic energy barrier).

302 Analysis of the TS thermodynamic properties of ligand
303 binding shows a high enthalpic energy barrier for Z80 and
304 ZM241385, counterbalanced by favourable entropic gains.
305 Visual inspection of the kinetic bottlenecks obtained using
306 the suMetaD protocol for these two small molecules (Fig. 5a,
307 b) shows ligand positions deep in the orthosteric site. The
308 high enthalpic barrier is linked to the displacement of most
309 of the water molecules, with stable interactions with the
310 protein orthosteric site then created. At the same time their
311 release to bulk results in an entropically favourable bind-
312 ing event. For KW3902 and XAC, the enthalpic TS binding
313 energy barriers decrease together with the entropic balanc-
314 ing effect. This is agreement with their kinetic bottlenecks
315 predicted close to the vestibule region (Fig. 5c, d), resulting

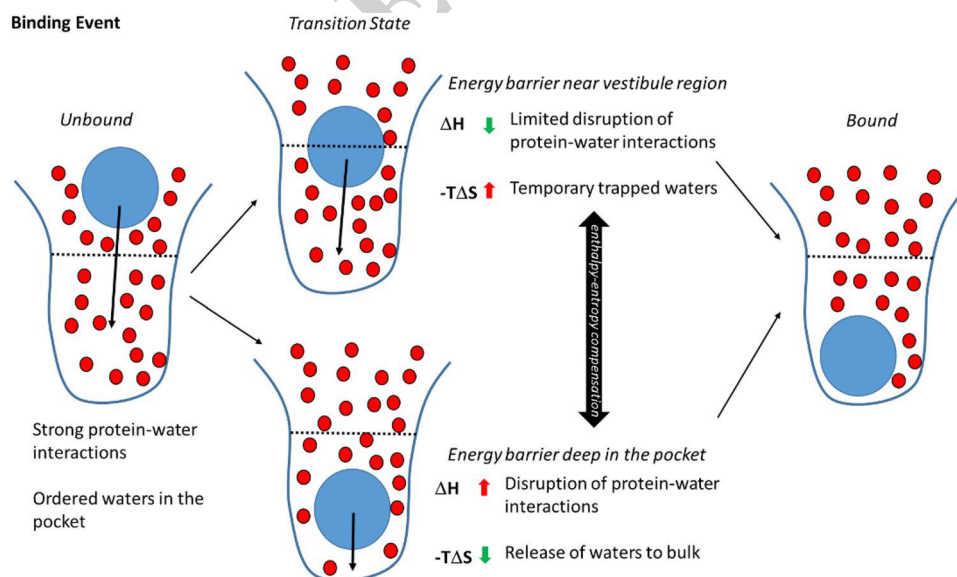


Fig. 3 Schematic overview of the two alternative transition state locations detected by the suMetaD protocol for the ligand binding event. The ligand is represented by a blue circle, waters by smaller red circles, the pocket by a blue line divided by a black dotted line in the orthosteric site (bottom half) and the vestibule region (top half). Starting from the unbound state (left) with strong protein–water inter-

actions and ordered waters the ligand reaches the bound state (right). Two alternative ligand locations corresponding to the transition state have been detected, the upper transition state showing the energy barrier is near the vestibule region and the lower one where it is deep in the orthosteric site. They are characterized by opposite enthalpic and entropic components related to the desolvation of the binding site

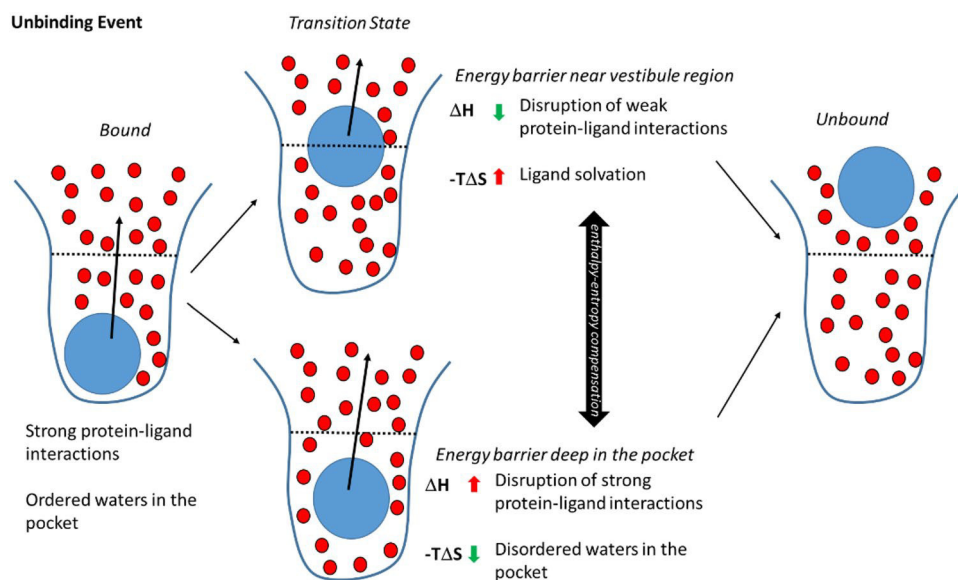


Fig. 4 Schematic overview of the two alternative transition state locations detected by the suMetaD protocol for the ligand unbinding event. As in Fig. 3, the ligand is represented by a blue circle, waters by smaller red circles, the pocket by a blue line divided by a black dotted line in the orthosteric site (bottom half) and the vestibule region (top half). Starting from the bound state (left) with strong protein–ligand interactions and ordered waters the ligand reaches the

unbound state (right). Two alternative ligand locations corresponding to the transition state have been detected: on the top, the energy barrier is near the vestibule region; on the bottom is deep in the orthosteric site. They are characterized by opposite enthalpic and entropic components related to the solvation of the binding site and of the small molecule

316 in the release to bulk of only part of the stable waters in the
 317 site. SPR data shows Z48 binding TS barrier characterized by both enthalpic and entropic components, while for
 318 DPCPX is only entropic. Visual inspection of their kinetic
 319 bottlenecks (Fig. 5e, f) shows binding positions in the ves-
 320 tibule region creating weak interactions with the receptor.
 321 These interactions can explain the low enthalpic component
 322 of the binding energy. Their location near the loops results
 323 in a large structured water network in the pocket that needs
 324 to be disrupted to allow the small molecule to reach the final
 325 bound state, causing a higher entropic barrier.
 326

327 Analysis of the TS thermodynamic properties of ligand
 328 unbinding shows a high enthalpic energy barrier for
 329 ZM241385 counterbalanced by a favourable entropic gain.
 330 The predicted position/conformation (Fig. 6a) for its unbind-
 331 ing kinetic bottleneck shows the ligand still tightly bound in
 332 the orthosteric site. In this pose it creates good interactions
 333 with the receptor, linked to the high experimental enthalpic
 334 barrier. The counterbalancing entropic component can be
 335 related to the flexible 4-ethylphenol tail sitting on top of
 336 the binding site and less ordered waters (compared to the
 337 bound conformation) at the interface between the protein
 338 and the small molecule. For the other ligands, solvation
 339 of non-polar hydrophobic saturated ring or aliphatic tails
 340 results in increasing unbinding entropic energy barriers. In
 341 Z80, XAC and Z48 transition states (Fig. 6b–d) the water
 342 network starts to act more like a lid on the extracellular side.

The solvent molecules create a complex web of hydrogen
 bond interactions hindering ligand unbinding. In KW3902
 (Fig. 6e), the bulky and hydrophobic saturated ring system
 touching the solvent increases further the unbinding entropic
 barrier. The predicted kinetic bottleneck positions for these
 ligands are between the bound state and the loops creating
 interactions with the receptor not as strong as ZM241385
 in its TS position. In particular, the predicted TS pose for
 DPCPX (Fig. 6f) is in the loop region close to several sol-
 vent molecules, creating a cage of H-bonds, resulting in a
 high entropic energy barrier for ligand unbinding.

Discussion

It is still challenging to understand ligand binding and
 unbinding kinetic properties at a molecular level. In general,
 transition state energy barriers correspond to kinetic bottle-
 neck positions and conformations the ligand needs to over-
 come to reach the final state. Their enthalpic and entropic
 components determine ligand *on* and *off* rates. TS enthalpy
 barriers are mainly linked to polar interactions among the
 ligand, the protein and the waters, while the entropic com-
 ponent is strongly related to changes in protein/ligand flex-
 ibility and solvation/desolvation effects. For the ligands
 considered in this study, the binding entropy barrier was
 found to be correlated to the number of temporary trapped

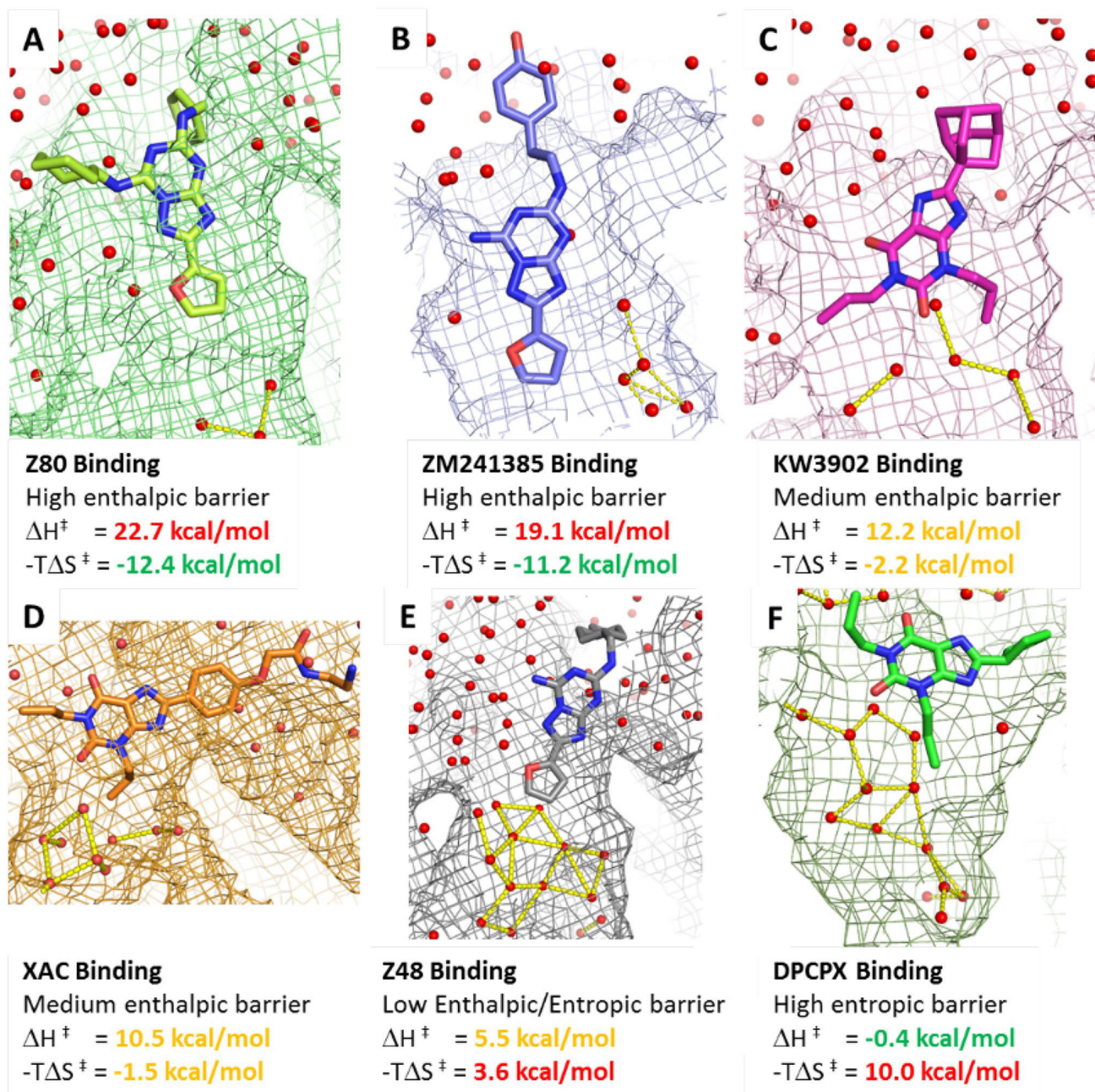


Fig. 5 Protein–ligand locations/conformations corresponding to the binding kinetic bottlenecks detected by the suMetaD protocol for the 6 small molecules considered in this study. The ligand is shown in stick representation, the pocket as a mesh surface and waters as small

spheres. Interactions among waters in the orthosteric site are shown as yellow dotted lines. The experimental energy of the enthalpic (ΔH^\ddagger) and entropic ($-T\Delta S^\ddagger$) components of the TS is reported

367 waters in the orthosteric site in the predicted energy barrier
368 position/conformation (Fig. 7). For the unbinding event the
369 TS entropic barrier was related to the number of waters in
370 the extracellular side of the receptor at less than 4 Å from
371 the ligand aliphatic carbon atoms (Fig. 7).

372 Using a molecular dynamics-based approach we have
373 been able to simulate the ligand binding and unbinding
374 events to extract possible low energy pathways linking the

docked ligand location to the extracellular side of the recep-
tor. Using a supervised MD algorithm the simulation explo-
ration is optimized to consider only directions compatible
with the desired binding or unbinding events. In parallel we
enhanced the conformational space sampling and we evalu-
ated the energy of the obtained hypothetical pathway using
metadynamics. Metadynamics allows the extraction of a
representative conformation of the system corresponding to

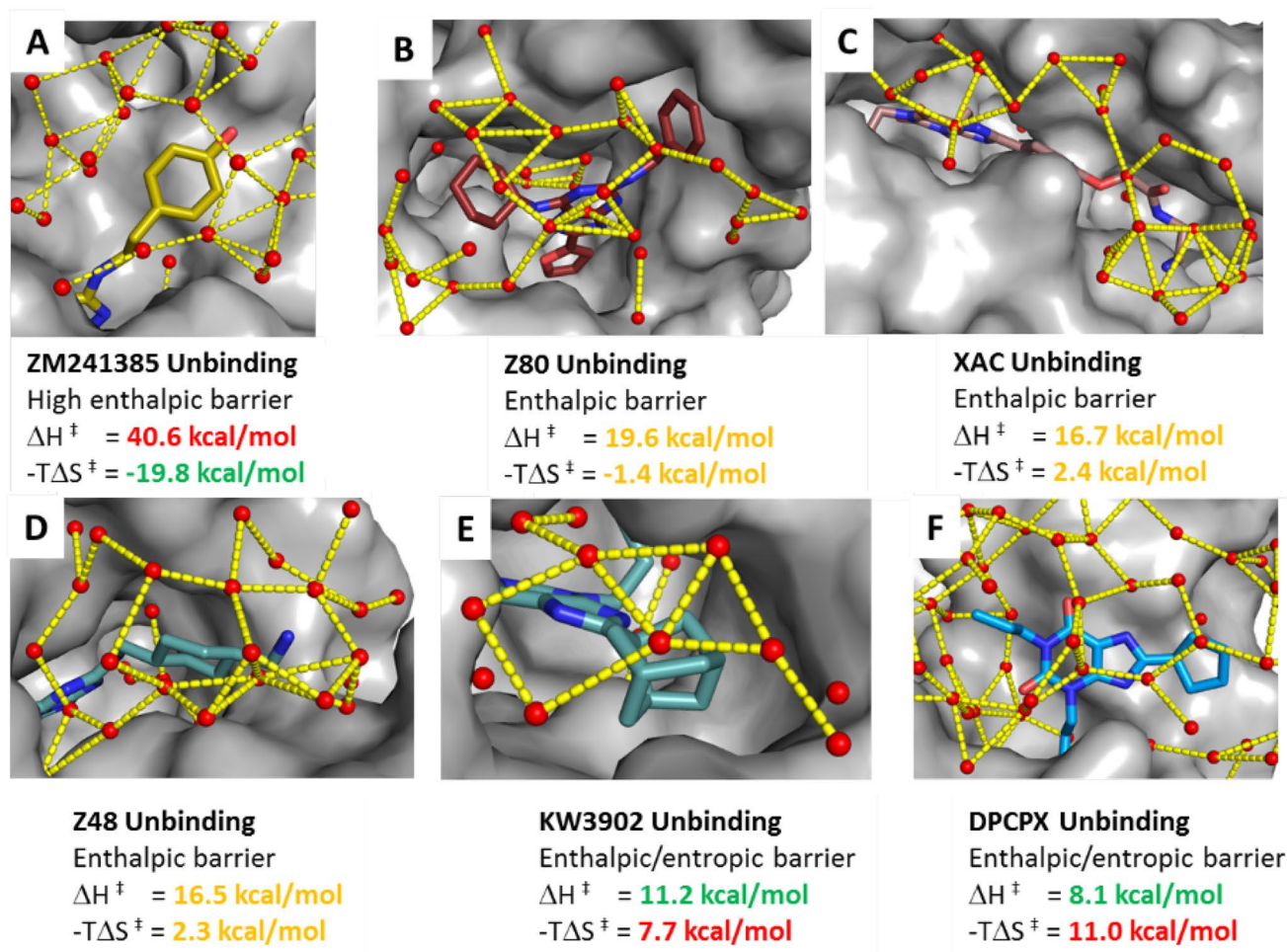


Fig. 6 Protein–ligand positions/conformations corresponding to the unbinding kinetic bottlenecks detected by the suMetaD protocol for the 6 small molecules considered in this study. The ligand is shown in stick representation, the pocket as solid grey surface and waters

as small spheres. Interactions among waters in the vestibule region near the ligand and among the extracellular loops are shown as yellow dotted lines. The experimental energy of the enthalpic (ΔH^\ddagger) and entropic ($-T\Delta S^\ddagger$) components of the TS is reported

383 the high energy barrier the ligand has to overcome to reach
 384 the target state. The resulting molecular details of the kinetic
 385 bottlenecks have been useful to generate testable working
 386 hypothesis to understand the key aspects of the ligand structure
 387 determining the *on* and *off* rates.

388 For the six ligands evaluated in this study their transition
 389 thermodynamic properties were linked in particular to
 390 the role of water molecules. During the binding event the
 391 ligand has to face a complex ordered water network in the
 392 pocket. Its ability to disrupt those interactions, resulting in
 393 the expulsion of waters into bulk solvent, determines if the
 394 TS conformation will be near the final bound state position
 395 or in the vestibule area, close to the extracellular loops. In
 396 the first case the barrier is mainly enthalpic, requiring the
 397 breaking of stable protein–waters interactions. In the second
 398 case it will be largely entropic, due to temporarily trapped
 399 waters in the pocket. These opposite energetic components

result in the enthalpy–entropy compensation effect we see
 experimentally for the six ligands.

It is possible to reach a similar conclusion from the analysis of the unbinding events. TS positions/conformations can be near the starting bound state position or in the vestibule area. In the former case the barrier is mainly enthalpic, requiring the breaking of strong interactions with the protein. In the latter case with a vestibule TS location, the kinetic bottleneck is instead mainly of an entropic nature, linked to the solvation of the ligand and the binding site.

In conclusion, several different aspects can play important roles affecting the transition state energy barrier that the small molecule has to overcome to reach the final state. The suMetaD method we developed and presented in this paper provides a useful tool to improve our understanding of the TS molecular details. It can help both to interpret structure-kinetic relationships and to make predictions for new molecules. The promising results obtained for the test

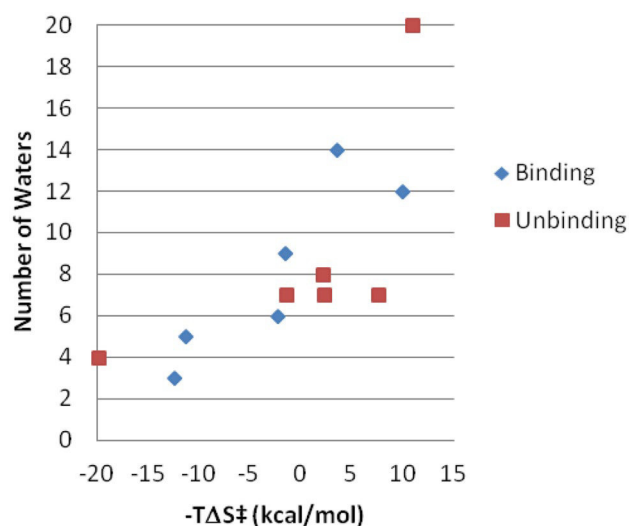


Fig. 7 Role of the solvent in the transition state entropic energy barrier. The experimental binding (blue) and unbinding (red) TS entropic barrier for the 6 ligands considered in this study is plotted on the X-axis. The Y-axis shows for the binding event (blue) the corresponding number of temporary trapped waters in the orthosteric site in the representative TS conformation. For the unbinding event (red), the Y-axis includes the number of waters in the extracellular side of the receptor at less than 4 Å from the ligand aliphatic carbon atoms in the representative TS conformation

418 set presented herein need now to be extended to a bigger
419 transition state thermodynamic datasets to fully prove the
420 general applicability of this approach.

421 Methods

422 Expression of A_{2A}R in insect cells

423 A_{2A} AR StaR 2 carrying a C-terminal deca His tag was
424 expressed in *Sf21* cells grown in ESF921 medium supple-
425 mented with 10% (v/v) FBS and 1% (v/v) Penicillin/Strep-
426 tomycin using the FastBac expression system (Invitrogen).
427 Cells were infected at a density of 2.5×10^6 cells/ml with
428 baculovirus at an approximate multiplicity of infection of
429 1. Cultures were grown at 27 °C and harvested 48 h post
430 infection.

431 Membrane preparation and protein purification

432 All subsequent purification steps were carried out at 4 °C. To
433 prepare membranes, 2 l of cells were re-suspended in PBS
434 buffer supplemented with cComplete Protease Inhibitor™
435 tablets (Roche) and 5 mM EDTA. Cells were disrupted by
436 micro-fluidizer at 60 PSI and membranes collected by ultra-
437 centrifugation at 204.7 k×g for 1 h. Membranes were washed
438 with PBS buffer supplemented with protease inhibitor tablets

and 500 mM NaCl, collected by ultracentrifugation and re- 439
suspended in 40 mM HEPES pH 7.5, 250 mM NaCl and 440
stored at - 80 °C. Just prior to solubilization membranes 441
were thawed, homogenized, supplemented with 10 μM 442
ZM24134 and incubated on a roller mixer for 60 min. 443
Membranes were solubilized with 1.5% (w/v) DM for 1 h, 444
insoluble material was removed by ultra-centrifugation 445
and the solubilized lysate batch bound to 5 ml of Ni-NTA 446
Superflow resin (Qiagen) for 3 h in the presence of 10 mM 447
imidazole. Resin was washed with a gradient of 10–50 mM 448
imidazole in 40 mM HEPES pH 7.5, 250 mM NaCl, 0.15% 449
(w/v) DM, and 10 μM ZM24134 over 35 column volumes 450
before bound material was eluted in a step with 245 mM imi- 451
dazole. Receptor was further purified by gel filtration (SEC) 452
in 40 mM HEPES pH 7.5, 150 mM NaCl, 0.15% (w/v) DM, 453
and 10 μM ZM24134. Receptor purity was analyzed using 454
SDS-PAGE and LC-MS, and receptor monodispersity was 455
assayed by analytical SEC. Protein concentration was deter- 456
mined using the receptor's calculated extinction coefficient 457
at 280 nm [$\epsilon_{280, \text{calc}} = 47,780 \text{ (mg/ml} \times \text{cm)}^{-1}$] and con- 458
firmed by quantitative amino acid analysis. 459

460 Assay of binding thermodynamics by SPR

461 SPR experiments were carried out on a Biacore T200 instru- 462
ment with a sensor chip NTA (GE Healthcare). The running 463
buffer was 10 mM phosphate, pH 7.4, 2.7 mM KCl, 137 mM 464
NaCl, 0.05 mM EDTA, 5% DMSO. A_{2A} AR was injected 465
over Ni-loaded chip NTA at 200 nM for 10 min at 10 °C 466
to obtain about 5000 resonance units (RU) of immobilised 467
receptor. Transition state thermodynamics was evaluated 468
using association and dissociation rate constants measured at 469
temperatures between 5 and 35 °C at 5 °C intervals. A series 470
of five twofold dilutions of the test compounds was injected 471
and the obtained sensorgrams were fitted to 1:1 interaction 472
model to obtain the rate constants. The temperature depend- 473
ence of the rate constants was fitted to Eyring equation using 474
Biacore T200 evaluation software to obtain enthalpy and 475
entropy of transition state formation.

476 suMetaD

477 For the ligands ZM241385, Z48 and Z80, the A_{2A} AR con- 478
formation was based on PDB:4E1Y (Liu et al. 2012), while 479
for the other ligands PDB:3REY (Doré et al. 2011) was used. 480
The fusion protein was removed from 4E1Y and the protein 481
sequence was modified to correspond to the construct used 482
in the SPR experiments using Prime (Jacobson et al. 2004) 483
(Schrödinger Release 2016-3). Receptors were prepared with 484
the Protein Preparation Wizard in Maestro (Schrödinger 485
Release 2016-3): the H-bond network has been optimized 486
through an exhaustive sampling of hydroxyl and thiol moie- 487
ties, tautomeric and ionic state of His and 180° rotations of

488 the terminal dihedral angle of amide groups of Asp and Gln.
 489 His264 has been considered to be protonated. The starting
 490 docking poses for Z48 and Z80 were based on ZM241385
 491 and refined using Glide (Friesner et al. 2004; Halgren et al.
 492 2004). For Z80 the rotameric state of H264 and E169 were
 493 modified to be comparable to the conformation of the cor-
 494 responding residues in the PDB 3PWH (Doré et al. 2011)
 495 A_{2A} AR crystal structure. The docking poses of DPCPX
 496 and KW3902 were based on XAC bound crystallographic
 497 conformation and refined using Glide (Friesner et al. 2004;
 498 Halgren et al. 2004). For these two ligands Y271^{7,36} rota-
 499 meric state was changed to be comparable to its conforma-
 500 tion in 4EIY.

501 The supervised metadynamics protocol (included in a
 502 single python script, suMetaD.py) uses as input the pro-
 503 tein PDB, and the bound conformations of the ligands (as
 504 SDF) and reasonable target ligand unbound positions near
 505 the extracellular side (also as SDF), at about 20 Å from the
 506 bound conformation. aMetaD.py protocol can be divided in
 507 the two steps: (1) system preparation and equilibration; (2)
 508 supervised metadynamics (suMetaD).

509 System preparation and equilibration

510 Every ligand-receptor complex is aligned to a reference
 511 (+Z corresponds to the extracellular side, -Z to the intra-
 512 cellular side, the membrane is in the XY plane). The sys-
 513 tem is equilibrated using the following molecular dynam-
 514 ics protocol. The AMBER99SB force field (ff) parameters
 515 (Lindorff-Larsen et al. 2010) were used for the protein and
 516 the GAFF ff (Wang et al. 2004) for the ligands using AM1-
 517 BCC partial charges (Jakalian et al. 2002). The system has
 518 been embedded in a triclinic box including an equilibrated
 519 membrane consisting of 256 DMPC (1,2-dimyristoyl-*sn*-
 520 glycerol-3-phosphocholine) lipids (Jämbeck and Lyubartsev
 521 2012) and 24,513 waters using g_membed (Wolf et al. 2010)
 522 in Gromacs. The SPC water model was used and ions were
 523 added to neutralize the system (final concentration 0.01 M).
 524 An energy minimization protocol based on 1000 steps steep-
 525 est-descent algorithm has been applied to the system. The
 526 membrane has been equilibrated using 0.5 ns MD simula-
 527 tion with a time step of 2.5 fs, using LINCS on all bonds
 528 and keeping the protein and ligand restrained applying a
 529 force of 100 kJ mol⁻¹ nm⁻¹. Lennard-Jones and Coulomb
 530 interactions were treated with a cut-off of 1.069 nm with
 531 particle-mesh Ewald electrostatics (PME) (Darden et al.
 532 1993). The MD has been executed in the NPT ensemble
 533 using v-rescale (Bussi et al. 2007) (tau_t = 0.5 ps) for the
 534 temperature coupling to maintain the temperature of 298 K
 535 and using Parrinello–Rahman (Parrinello and Rahman 1981)
 536 (tau_p = 10.0 ps) for the semi-isotropic pressure coupling
 537 to maintain the pressure of 1.013 bar. Without applying any
 538 positional restraints, the system has been minimized for 200

539 steps using the steepest-descent algorithm and equilibrated
 540 using MD using the same settings described above, but with
 541 a time step of 2 fs and increasing the temperature from 29.8
 542 to 298 K in 10 steps (9 steps of 30 ps and the last one of
 543 300 ps).

Supervised metadynamics (suMetaD) 544

545 The metadynamics (Barducci et al. 2011) protocol exploits
 546 a generic path collective variable (CV) (Branduardi et al.
 547 2007) generated using the RMSD between the starting
 548 ligand bound state and a ligand position corresponding to
 549 the original starting ligand location translated 3 Å on the
 550 X-axis. Two path CVs have been considered: one defining
 551 the RMSD position on this path (*s*) and the other the RMSD
 552 distance from the path (*z*) using lambda = 20. The same
 553 MD settings used during the final system equilibration at
 554 298 K are used for the suMetaD protocol. For the meta-
 555 dynamics algorithm the following settings have been used:
 556 initial energy bias Gaussian height of 0.25 kcal/mol with a
 557 deposition frequency of 1 ps. The width of the Gaussians
 558 was 0.01 Å. The suMetaD protocol is divided in two con-
 559 secutive parts:

- 560 1. The ligand unbinding event is simulated first using a
 561 maximum of 200 metadynamics steps of 50 ps each
 562 (always writing to the same COLVAR file using the
 563 RESTART keyword) for a total of maximum 10 ns. The
 564 supervised algorithm is implemented in the following
 565 way: after every step if the RMSD from the target ligand
 566 position is decreased the next step starts from the end of
 567 the previous step, otherwise from the beginning of the
 568 previous step assigning new random atom velocities. If
 569 the ligand reaches a distance of 15 Å from the bound
 570 position the simulation is stopped.
- 571 2. The final output coordinates from the ligand unbinding
 572 simulation is used as a starting conformation for ligand
 573 binding simulation. As before, a maximum of 200 meta-
 574 dynamics steps of 50 ps each are simulated. A compa-
 575 rable supervised algorithm is used, but the RMSD from
 576 the target bound ligand position is used. If the ligand
 577 reaches a distance of 3 Å from the bound position the
 578 simulation is stopped.

579 The final results included for the analysis are: (1) the
 580 binding/unbinding trajectories; (2) the metadynamics energy
 581 profile as function of the bound state RMSD; (3) the confor-
 582 mation corresponding to the highest energy barrier (based on
 583 the metadynamics bias energy deposition) for the unbinding
 584 and binding event.

585 **References**

- 586 Barducci A, Bussi G, Parrinello M (2008) Well-tempered meta-
587 dynamics: a smoothly converging and tunable free-energy
588 method. *Phys Rev Lett* 100:020603. [https://doi.org/10.1103/](https://doi.org/10.1103/PhysRevLett.100.020603)
589 [PhysRevLett.100.020603](https://doi.org/10.1103/PhysRevLett.100.020603)
- 590 Barducci A, Bonomi M, Parrinello M (2011) Metadynamics: meta-
591 dynamics. *Wiley Interdiscip Rev Comput Mol Sci* 1:826–843.
592 <https://doi.org/10.1002/wcms.31>
- 593 Borea PA, Varani K, Gessi S, Merighi S, Dal Piaz A, Gilli P et al
594 (2004) Receptor binding thermodynamics at the neuronal nico-
595 tinic receptor. *Curr Top Med Chem* 4:361–368
- 596 Bortolato A, Deflorian F, Weiss DR, Mason JS (2015) Decoding
597 the role of water dynamics in ligand-Protein unbinding: CRF 1
598 R as a test case. *J Chem Inf Model* 55:1857–1866. [https://doi.](https://doi.org/10.1021/acs.jcim.5b00440)
599 [org/10.1021/acs.jcim.5b00440](https://doi.org/10.1021/acs.jcim.5b00440)
- 600 Branduardi D, Gervasio FL, Parrinello M (2007) From A to B
601 in free energy space. *J Chem Phys* 126:54103. [https://doi.](https://doi.org/10.1063/1.2432340)
602 [org/10.1063/1.2432340](https://doi.org/10.1063/1.2432340)
- 603 Branduardi D, Bussi G, Parrinello M (2012) Metadynamics with adap-
604 tive Gaussians. *J Chem Theory Comput* 8:2247–2254. [https://doi.](https://doi.org/10.1021/ct3002464)
605 [org/10.1021/ct3002464](https://doi.org/10.1021/ct3002464)
- 606 Bui JM, Henchman RH, McCammon JA (2003) The dynamics of ligand
607 barrier crossing inside the acetylcholinesterase gorge. *Biophys J*
608 85:2267–2272. [https://doi.org/10.1016/S0006-3495\(03\)74651-7](https://doi.org/10.1016/S0006-3495(03)74651-7)
- 609 Bussi G, Donadio D, Parrinello M (2007) Canonical sampling
610 through velocity rescaling. *J Chem Phys* 126:14101. [https://doi.](https://doi.org/10.1063/1.2408420)
611 [org/10.1063/1.2408420](https://doi.org/10.1063/1.2408420)
- 612 Carpenter B, Nehmé R, Warne T, Leslie AGW, Tate CG (2016) Struc-
613 ture of the adenosine A_{2A} receptor bound to an engineered G
614 protein. *Nature* 536:104–107. <https://doi.org/10.1038/nature18966>
- 615 Congreve M, Andrews SP, Doré AS, Hollenstein K, Hurrell E, Lang-
616 mead CJ et al (2012) Discovery of 1,2,4-triazine derivatives as
617 adenosine A_{2A} antagonists using structure based drug design. *J*
618 *Med Chem* 55:1898–1903. <https://doi.org/10.1021/jm201376w>
- 619 Copeland RA (2015) The drug–target residence time model: a 10-year
620 retrospective. *Nat Rev Drug Discov* 15:87–95. [https://doi.](https://doi.org/10.1038/nrd.2015.18)
621 [org/10.1038/nrd.2015.18](https://doi.org/10.1038/nrd.2015.18)
- 622 Copeland RA, Pompliano DL, Meek TD (2006) Drug–target residence
623 time and its implications for lead optimization. *Nat Rev Drug*
624 *Discov* 5:730–739. <https://doi.org/10.1038/nrd2082>
- 625 Cuzzolin A, Sturlese M, Deganutti G, Salmasso V, Sabbadin D, Cian-
626 cetta A et al (2016) Deciphering the complexity of ligand-protein
627 recognition pathways using supervised molecular dynamics
628 (SuMD) simulations. *J Chem Inf Model* 56:687–705. [https://doi.](https://doi.org/10.1021/acs.jcim.5b00702)
629 [org/10.1021/acs.jcim.5b00702](https://doi.org/10.1021/acs.jcim.5b00702)
- 630 Dahl G, Akerud T (2013) Pharmacokinetics and the drug–target resi-
631 dence time concept. *Drug Discov Today* 18:697–707. [https://doi.](https://doi.org/10.1016/j.drudis.2013.02.010)
632 [org/10.1016/j.drudis.2013.02.010](https://doi.org/10.1016/j.drudis.2013.02.010)
- 633 Darden T, York D, Pedersen L (1993) Particle mesh Ewald: an $N \log(N)$
634 method for Ewald sums in large systems. *J Chem Phys* 98:10089–
635 10092. <https://doi.org/10.1063/1.464397>
- 636 Doré AS, Robertson N, Errey JC, Ng I, Hollenstein K, Tehan B et al
637 (2011) Structure of the adenosine A_{2A} receptor in complex
638 with ZM241385 and the xanthines XAC and caffeine. *Struc-*
639 *ture* 19:1283–1293. <https://doi.org/10.1016/j.str.2011.06.014>
- 640 Dror RO, Pan AC, Arlow DH, Borhani DW, Maragakis P, Shan Y et al
641 (2011) Pathway and mechanism of drug binding to G-protein-
642 coupled receptors. *Proc Natl Acad Sci* 108:13118–13123. [https://](https://doi.org/10.1073/pnas.1104614108)
643 doi.org/10.1073/pnas.1104614108
- 644 Du X, Li Y, Xia Y-L, Ai S-M, Liang J, Sang P et al (2016) Insights into
645 protein-ligand interactions: mechanisms, models, and methods. *Int*
646 *J Mol Sci* 17:144. <https://doi.org/10.3390/ijms17020144>
- 647 Federico S, Paoletta S, Cheong SL, Pastorin G, Cacciari B, Stragliotto
648 S et al (2011) Synthesis and biological evaluation of a new series
649 of 1,2,4-triazolo[1,5-*a*]-1,3,5-triazines as human A_{2A} adenosine
650 receptor antagonists with improved water solubility. *J Med Chem*
651 54:877–889. <https://doi.org/10.1021/jm101349u>
- Federico S, Ciancetta A, Porta N, Redenti S, Pastorin G, Cacciari B
652 et al (2016) 5,7-Disubstituted-[1,2,4]triazolo[1,5-*a*][1,3,5]triaz-
653 ines as pharmacological tools to explore the antagonist selectiv-
654 ity profiles toward adenosine receptors. *Eur J Med Chem*
655 108:529–541. <https://doi.org/10.1016/j.ejmech.2015.12.019>
- Fink JS, Weaver DR, Rivkees SA, Peterfreund RA, Pollack AE, Adler
656 EM et al (1992) Molecular cloning of the rat A₂ adenosine recep-
657 tor: selective co-expression with D₂ dopamine receptors in rat
658 striatum. *Brain Res Mol Brain Res* 14:186–195
- Frederick KK, Marlow MS, Valentine KG, Wand AJ (2007) Confor-
659 mational entropy in molecular recognition by proteins. *Nature*
660 448:325–329. <https://doi.org/10.1038/nature05959>
- Friesner RA, Banks JL, Murphy RB, Halgren TA, Klicic JJ, Mainz
661 DT et al (2004) Glide: a new approach for rapid, accurate dock-
662 ing and scoring 1 method and assessment of docking accuracy.
663 *J Med Chem* 47:1739–1749. <https://doi.org/10.1021/jm0306430>
- Fukunishi H, Watanabe O, Takada S (2002) On the Hamiltonian rep-
664 lica exchange method for efficient sampling of biomolecular sys-
665 tems: application to protein structure prediction. *J Chem Phys*
666 116:9058–9067. <https://doi.org/10.1063/1.1472510>
- Gervasio FL, Laio A, Parrinello M (2005) Flexible docking in solution
667 using metadynamics. *J Am Chem Soc* 127:2600–2607. [https://doi.](https://doi.org/10.1021/ja0445950)
668 [org/10.1021/ja0445950](https://doi.org/10.1021/ja0445950)
- Ghosh E, Kumari P, Jaiman D, Shukla AK (2015) Methodological
669 advances: the unsung heroes of the GPCR structural revolution.
670 *Nat Rev Mol Cell Biol* 16:69–81. <https://doi.org/10.1038/nrm3933>
- Guo D, Pan AC, Dror RO, Mocking T, Liu R, Heitman LH et al (2016)
671 Molecular basis of ligand dissociation from the adenosine A_{2A}
672 receptor. *Mol Pharmacol* 89:485–491. [https://doi.org/10.1124/](https://doi.org/10.1124/mol.115.102657)
673 [mol.115.102657](https://doi.org/10.1124/mol.115.102657)
- Guo D, Heitman LH, IJzerman AP (2017) Kinetic aspects of the inter-
674 action between ligand and G protein-coupled receptor: the case
675 of the adenosine receptors. *Chem Rev* 117:38–66. [https://doi.](https://doi.org/10.1021/acs.chemrev.6b00025)
676 [org/10.1021/acs.chemrev.6b00025](https://doi.org/10.1021/acs.chemrev.6b00025)
- Halgren TA, Murphy RB, Friesner RA, Beard HS, Frye LL, Pollard
677 WT et al (2004) Glide: a new approach for rapid, accurate dock-
678 ing and scoring 2 enrichment factors in database screening. *J Med*
679 *Chem* 47:1750–1759. <https://doi.org/10.1021/jm030644s>
- Hamelberg D, Mongan J, McCammon JA (2004) Accelerated molecu-
680 lar dynamics: a promising and efficient simulation method for
681 biomolecules. *J Chem Phys* 120:11919–11929. [https://doi.](https://doi.org/10.1063/1.1755656)
682 [org/10.1063/1.1755656](https://doi.org/10.1063/1.1755656)
- Hino T, Arakawa T, Iwanari H, Yurugi-Kobayashi T, Ikeda-Suno C,
683 Nakada-Nakura Y et al (2012) G-protein-coupled receptor inac-
684 tivation by an allosteric inverse-agonist antibody. *Nature*. [https://](https://doi.org/10.1038/nature10750)
685 doi.org/10.1038/nature10750
- Hothersall JD, Brown AJ, Dale I, Rawlins P (2016) Can residence
686 time offer a useful strategy to target agonist drugs for sustained
687 GPCR responses? *Drug Discov Today* 21:90–96. [https://doi.](https://doi.org/10.1016/j.drudis.2015.07.015)
688 [org/10.1016/j.drudis.2015.07.015](https://doi.org/10.1016/j.drudis.2015.07.015)
- Hulme EC, Trevethick MA (2010) Ligand binding assays at equi-
689 librium: validation and interpretation: equilibrium binding
690 assays. *Br J Pharmacol* 161:1219–1237. [https://doi.](https://doi.org/10.1111/j.1476-5381.2009.00604.x)
691 [org/10.1111/j.1476-5381.2009.00604.x](https://doi.org/10.1111/j.1476-5381.2009.00604.x)
- Isralewitz B, Gao M, Schulten K (2001) Steered molecular dynam-
692 ics and mechanical functions of proteins. *Curr Opin Struct Biol*
693 11:224–230
- Jaakola V-P, Griffith MT, Hanson MA, Cherezov V, Chien EYT, Lane
694 JR et al (2008) The 26 angstrom crystal structure of a human A_{2A}
695 adenosine receptor bound to an antagonist. *Science* 322:1211–
696 1217. <https://doi.org/10.1126/science.1164772>

713 Jacobson KA, Gao Z-G (2006) Adenosine receptors as therapeutic targets. *Nat Rev Drug Discov* 5:247–264. <https://doi.org/10.1038/nrd1983>

714

715 Jacobson MP, Pincus DL, Rapp CS, Day TJF, Honig B, Shaw DE et al (2004) A hierarchical approach to all-atom protein loop prediction. *Proteins Struct Funct Bioinform* 55:351–367. <https://doi.org/10.1002/prot.10613>

716

717

718

719

720 Jakalian A, Jack DB, Bayly CI (2002) Fast, efficient generation of high-quality atomic charges AM1-BCC model: II parameterization and validation. *J Comput Chem* 23:1623–1641. <https://doi.org/10.1002/jcc.10128>

721

722

723

724 Jämbeck JPM, Lyubartsev AP (2012) Derivation and systematic validation of a refined all-atom force field for phosphatidylcholine lipids. *J Phys Chem B* 116:3164–3179. <https://doi.org/10.1021/jp212503e>

725

726

727

728 Kenakin T, Christopoulos A (2012) Signalling bias in new drug discovery: detection, quantification and therapeutic impact. *Nat Rev Drug Discov* 12:205–216. <https://doi.org/10.1038/nrd3954>

729

730

731 Laio A, Parrinello M (2002) Escaping free-energy minima. *Proc Natl Acad Sci* 99:12562–12566. <https://doi.org/10.1073/pnas.202427399>

732

733

734 Laio A, Rodriguez-Fortea A, Gervasio FL, Ceccarelli M, Parrinello M (2005) Assessing the accuracy of metadynamics. *J Phys Chem B* 109:6714–6721. <https://doi.org/10.1021/jp045424k>

735

736

737 Lebon G, Warne T, Edwards PC, Bennett K, Langmead CJ, Leslie AGW et al (2011) Agonist-bound adenosine A2A receptor structures reveal common features of GPCR activation. *Nature* 474:521–525. <https://doi.org/10.1038/nature10136>

738

739

740

741 Lebon G, Edwards PC, Leslie AGW, Tate CG (2015) Molecular determinants of CGS21680 binding to the human adenosine A2A receptor. *Mol Pharmacol* 87:907–915. <https://doi.org/10.1124/mol.114.097360>

742

743

744

745 Li W (2005) Possible pathway(s) of testosterone egress from the active site of cytochrome P450 2B1: a steered molecular dynamics simulation. *Drug Metab Dispos* 33:910–919. <https://doi.org/10.1124/dmd.105.004200>

746

747

748

749 Lindorff-Larsen K, Piana S, Palmo K, Maragakis P, Klepeis JL, Dror RO et al (2010) Improved side-chain torsion potentials for the Amber ff99SB protein force field. *Proteins*. <https://doi.org/10.1002/prot.22711>

750

751

752

753 Liu W, Chun E, Thompson AA, Chubukov P, Xu F, Katritch V et al (2012) Structural basis for allosteric regulation of GPCRs by sodium ions. *Science* 337:232–236. <https://doi.org/10.1126/science.1219218>

754

755

756

757 Luitz MP, Zacharias M (2014) Protein-ligand docking using Hamiltonian replica exchange simulations with soft core potentials. *J Chem Inf Model* 54:1669–1675. <https://doi.org/10.1021/ci500296f>

758

759

760

761 Marchi M, Ballone P (1999) Adiabatic bias molecular dynamics: a method to navigate the conformational space of complex molecular systems. *J Chem Phys* 110:3697–3702. <https://doi.org/10.1063/1.478259>

762

763

764

765 Mollica L, Decherchi S, Zia SR, Gaspari R, Cavalli A, Rocchia W (2015) Kinetics of protein-ligand unbinding via smoothed potential molecular dynamics simulations. *Sci Rep* 5:11539. <https://doi.org/10.1038/srep11539>

766

767

768

769 Mollica L, Theret I, Antoine M, Perron-Sierra F, Charton Y, Fourquez J-M et al (2016) Molecular dynamics simulations and kinetic measurements to estimate and predict protein-ligand residence times. *J Med Chem* 59:7167–7176. <https://doi.org/10.1021/acs.jmedchem.6b00632>

770

771

772

773

774 Nguyen ATN, Baltos J-A, Thomas T, Nguyen TD, Munoz LL, Gregory KJ et al (2016) Extracellular loop 2 of the adenosine A1 receptor has a key role in orthosteric ligand affinity and agonist efficacy. *Mol Pharmacol* 90:703–714. <https://doi.org/10.1124/mol.116.105007>

775

776

777

778

Pan AC, Borhani DW, Dror RO, Shaw DE (2013) Molecular determinants of drug–receptor binding kinetics. *Drug Discov Today* 18:667–673. <https://doi.org/10.1016/j.drudis.2013.02.007>

Parrinello M, Rahman A (1981) Polymorphic transitions in single crystals: a new molecular dynamics method. *J Appl Phys* 52:7182–7190. <https://doi.org/10.1063/1.328693>

Patel JS, Berteotti A, Ronsisvalle S, Rocchia W, Cavalli A (2014) Steered molecular dynamics simulations for studying protein-ligand interaction in cyclin-dependent kinase 5. *J Chem Inf Model* 54:470–480. <https://doi.org/10.1021/ci4003574>

Pierce LCT, Salomon-Ferrer R, de Augusto Oliveira F, McCammon JA, Walker RC (2012) Routine access to millisecond time scale events with accelerated molecular dynamics. *J Chem Theory Comput* 8:2997–3002. <https://doi.org/10.1021/ct300284c>

Polosa R, Blackburn MR (2009) Adenosine receptors as targets for therapeutic intervention in asthma and chronic obstructive pulmonary disease. *Trends Pharmacol Sci* 30:528–535. <https://doi.org/10.1016/j.tips.2009.07.005>

Radić Z, Kirchhoff PD, Quinn DM, McCammon JA, Taylor P (1997) Electrostatic influence on the kinetics of ligand binding to acetylcholinesterase distinctions between active center ligands and fasciculin. *J Biol Chem* 272:23265–23277

Rich RL, Myszkowski DG (2009) Grading the commercial optical biosensor literature—Class of 2008: “The Mighty Binders”. *J Mol Recognit* 23:1–64. <https://doi.org/10.1002/jmr.1004>

Rich RL, Errey J, Marshall F, Myszkowski DG (2011) Biacore analysis with stabilized G-protein-coupled receptors. *Anal Biochem* 409:267–272. <https://doi.org/10.1016/j.ab.2010.10.008>

Richardson PJ, Kase H, Jenner PG (1997) Adenosine A2A receptor antagonists as new agents for the treatment of Parkinson’s disease. *Trends Pharmacol Sci* 18:338–344

Rivera-Oliver M, Díaz-Ríos M (2014) Using caffeine and other adenosine receptor antagonists and agonists as therapeutic tools against neurodegenerative diseases: a review. *Life Sci* 101:1–9. <https://doi.org/10.1016/j.lfs.2014.01.083>

Roos H, Karlsson R, Nilshans H, Persson A (1998) Thermodynamic analysis of protein interactions with biosensor technology. *J Mol Recognit* 11:204–210. [https://doi.org/10.1002/\(SICI\)1099-1352\(199812\)11:1/6<204::AID-JMR424>3.0.CO;2-T](https://doi.org/10.1002/(SICI)1099-1352(199812)11:1/6<204::AID-JMR424>3.0.CO;2-T)

Sabbadin D, Moro S (2014) Supervised molecular dynamics (SuMD) as a helpful tool to depict GPCR–ligand recognition pathway in a nanosecond time scale. *J Chem Inf Model* 54:372–376. <https://doi.org/10.1021/ci400766b>

Sahlan M, Zako T, Tai PT, Ohtaki A, Noguchi K, Maeda M et al (2010) Thermodynamic characterization of the interaction between pre-foldin and group II chaperonin. *J Mol Biol* 399:628–636. <https://doi.org/10.1016/j.jmb.2010.04.046>

Schmidtke P, Luque FJ, Murray JB, Barril X (2011) Shielded hydrogen bonds as structural determinants of binding kinetics: application in drug design. *J Am Chem Soc* 133:18903–18910. <https://doi.org/10.1021/ja207494u>

Segala E, Guo D, Cheng RKY, Bortolato A, Deflorian F, Doré AS et al (2016) Controlling the dissociation of ligands from the adenosine A_{2A} receptor through modulation of salt bridge strength. *J Med Chem* 59:6470–6479. <https://doi.org/10.1021/acs.jmedchem.6b00653>

Seibt BF, Schiedel AC, Thimm D, Hinz S, Sherbiny FF, Müller CE (2013) The second extracellular loop of GPCRs determines subtype-selectivity and controls efficacy as evidenced by loop exchange study at A2 adenosine receptors. *Biochem Pharmacol* 85:1317–1329. <https://doi.org/10.1016/j.bcp.2013.03.005>

Shaw DE, Dror RO, Salmon JK, Grossman JP, Mackenzie KM, Bank JA et al (2009) Millisecond-scale molecular dynamics simulations on Anton. In: *proc. conf. high perform. Comput Netw Storage Anal SC 09 no. c: 1–11*

Author Proof

- 844 Shepherd CA, Hopkins AL, Navratilova I (2014) Fragment screening by
845 SPR and advanced application to GPCRs. *Prog Biophys Mol Biol*
846 116:113–123. <https://doi.org/10.1016/j.pbiomolbio.2014.09.008>
- 847 Sinko W, Miao Y, de Oliveira CAF, McCammon JA (2013) Population
848 based reweighting of scaled molecular dynamics. *J Phys Chem B*
849 117:12759–12768. <https://doi.org/10.1021/jp401587e>
- 850 Stanley N, Pardo L, De Fabritiis G (2016) The pathway of ligand entry
851 from the membrane bilayer to a lipid G protein-coupled receptor.
852 *Sci Rep* 6:22639. <https://doi.org/10.1038/srep22639>
- 853 Stone TW, Ceruti S, Abbracchio MP (2009) Adenosine receptors and
854 neurological disease: neuroprotection and neurodegeneration.
855 In: Wilson CN, Mustafa SJ (eds) *Adenosine receptors in health*
856 *and disease*, vol 193. Springer, Berlin, pp 535–587. https://doi.org/10.1007/978-3-540-89615-9_17
- 857 Torrie GM, Valleau JP (1977) Nonphysical sampling distributions in
858 Monte Carlo free-energy estimation: umbrella sampling. *J Comput*
859 *Phys* 23:187–199. [https://doi.org/10.1016/0021-9991\(77\)90121-8](https://doi.org/10.1016/0021-9991(77)90121-8)
- 860 Vauquelin G, Bostoen S, Vanderheyden P, Seeman P (2012) Clozapine,
861 atypical antipsychotics, and the benefits of fast-off D2 dopamine
862 receptor antagonism. *Naunyn Schmiedebergs Arch Pharmacol* 385:337–372. <https://doi.org/10.1007/s00210-012-0734-2>
- 863 Wang J, Wolf RM, Caldwell JW, Kollman PA, Case DA (2004) Devel-
864 opment and testing of a general amber force field. *J Comput Chem*
865 25:1157–1174. <https://doi.org/10.1002/jcc.20035>
- 866 Wang K, Chodera JD, Yang Y, Shirts MR (2013) Identifying ligand
867 binding sites and poses using GPU-accelerated Hamiltonian rep-
868 lica exchange molecular dynamics. *J Comput Aided Mol Des*
869 27:989–1007. <https://doi.org/10.1007/s10822-013-9689-8>
- 870 Wolf MG, Hoefling M, Aponte-Santamaría C, Grubmüller H, Groenhof
871 G (2010) g_membed: efficient insertion of a membrane protein
872 into an equilibrated lipid bilayer with minimal perturbation. *J*
873 *Comput Chem* 31:2169–2174. <https://doi.org/10.1002/jcc.21507>
- 874 Xu F, Wu H, Katritch V, Han GW, Jacobson KA, Gao Z-G et al (2011)
875 Structure of an agonist-bound human A2A adenosine receptor.
876 *Science* 332:322–327. <https://doi.org/10.1126/science.1202793>
- 877 Yu R, Tabassum N, Jiang T (2016) Investigation of α -conotoxin
878 unbinding using umbrella sampling. *Bioorg Med Chem Lett*
879 26:1296–1300. <https://doi.org/10.1016/j.bmcl.2016.01.013>
- 880
881

Journal:	40203
Article:	37

Author Query Form

Please ensure you fill out your response to the queries raised below and return this form along with your corrections

Dear Author

During the process of typesetting your article, the following queries have arisen. Please check your typeset proof carefully against the queries listed below and mark the necessary changes either directly on the proof/online grid or in the 'Author's response' area provided below

Query	Details Required	Author's Response
AQ1	Kindly check and confirm the affiliation [2] is correctly processed.	
AQ2	Please confirm the section headings are correctly identified.	